DOI: 10.24850/j-tyca-13-05-04

Articles

Estimation of chlorophyll-a in urban lakes using drones

Estimación de clorofila-a en lagos urbanos mediante el uso de drones

Myrna Nevárez[1], ORCID: https://orcid.org/0000-0003-0325-2900

Mario Sigala[2], ORCID: https://orcid.org/0000-0001-7501-9206

[1]Universidad Autónoma de Chihuahua, Chihuahua, México, mcnevarez@uach.mx

[2]Universidad Autónoma de Chihuahua, Chihuahua, México, mario.alberto.sigala@gmail.com

Corresponding author: Myrna Nevárez, mcnevarez@uach.mx

Abstract

Urban lakes provide significant ecological and societal benefits, but they are compromised by anthropogenic activities when there are insufficient protection and monitoring programs. Several problems affect these water bodies, and eutrophication is one of the more significant issues. One of the indicators to estimate eutrophication is the chlorophyll-a

concentration in water (Chl-a), determined by analytical methods using fluorophotometry, spectrophotometry, and high-performance liquid chromatography (HPLC). In recent decades remote sensing of Chl-a in water bodies used satellite and airborne-based sensors. Still, those systems are inadequate for monitoring most urban lakes due to spatial and spectral resolution limitations, problems in modeling atmospheric corrections, and issues related to the removal of effects of other components in the water column. The methodology presented here estimated Chl-a content sensing sun-induced fluorescence (SIF) at the Fraunhofer line Hα (656.3 nm) and correlated the results to the concentrations reported by an external laboratory using fluorophotometry methods. The system used in this investigation has a georeferenced imaging system, an optical narrow-band filter (NBF), and a drone. The results of this investigation indicated that sensing at the Hα Fraunhofer line and a simple linear regression estimated better content of Chl-a in water compared to other studies measuring SIF at different Fraunhofer lines.

Keywords: Chlorophyll-a, drone, remote sensing, eutrophication.

Resumen

Los lagos urbanos brindan importantes beneficios ecológicos y sociales, pero se ven comprometidos por las actividades antrópicas cuando los programas de protección y monitoreo son insuficientes. Varios problemas afectan a estos cuerpos de agua, siendo la eutrofización uno

de los más importantes. Uno de los indicadores para estimar la eutrofización es la concentración de clorofila-a en agua (Chl-a), determinada por métodos analíticos utilizando fluorofotometría, espectrofotometría y cromatografía líquida de alta resolución (HPLC). En las últimas décadas, la detección remota de Chl-a en cuerpos de agua empleó sensores satelitales y aéreos, pero tales sistemas son inadecuados para monitorear la mayoría de los lagos urbanos debido a limitaciones en la resolución espacial y espectral, además de presentar problemas tanto en el modelado de correcciones atmosféricas como con la eliminación de los efectos de otros componentes en la columna de agua. La metodología aquí presentada estimó el contenido de Chl-a que detecta la fluorescencia inducida por el Sol (SIF) en la línea Fraunhofer Hα (656.3 nm) y correlacionó los resultados con las concentraciones informadas por un laboratorio externo usando métodos de fluorofotometría. El sistema aplicado en esta investigación cuenta con un sistema de imágenes georreferenciadas, un filtro óptico de banda estrecha (NBF) y un dron. Los resultados de la investigación indicaron que con la detección de SIF en la línea de Fraunhofer Hα y una regresión lineal simple se estimó mejor contenido de Chl-a en el agua, comparado con otros estudios que emplearon otras líneas de Fraunhofer.

Palabras clave: clorofila-a, dron, detección remota, eutrofización.

Received: 11/08/2020

Accepted: 11/06/2021

Tecnología y Ciencias del Agua

OPEN ACCESS

Check for updates

Introduction

Small lakes provide important ecological services, as they play roles in the water cycle, nutrient cycles, and climate regulation and are an adequate habitat for biodiversity. They also act as reservoirs for agricultural activities, fishery products, and areas for leisure and recreational activities (Wondie, 2018) and increase the land value and wellness of residents (Natarajan, Hagare, & Maheshwari, 2018). When combined with the inadequate management of urban lakes, anthropogenic activities negatively impact their ecosystem services (Chen *et al*., 2017). Urban lakes are strongly affected by developmental activities (Henny & Meutia, 2014) and are being eutrophicated, which requires complicated, long-term, and expensive environmental recovery (Vásquez & De-Rezende, 2018). The degradation of lake ecosystems is often aggravated by limited monitoring and diagnostic programs (Khorasani, Kerachian, & Malakpour-Estalakia, 2018). Therefore, we must develop effective methods of managing such ecosystems (Zhang *et al*., 2018) and establish periodic monitoring programs for their preservation and sustainability (Plisnier, Nshombo, Mgana, & Ntakimazi,

Tecnología y ciencias del agua, ISSN 2007-2422, 13(5), 101-135. DOI: 10.24850/j-tyca-13-05-04

2018). Studies have reported that chlorophyll-a (Chl-a) is a good indicator of eutrophication in lakes and oceans (EPA, 2000). Methods for measuring Chl-a have been established by the Environmental Protection Agency (EPA) of the USA, as follows: Method 445.0 - In-vitro determination of chlorophyll-a and pheophytin-a in marine and freshwater algae by fluorescence (Arar & Collins, 1997); Method 446.0 - In-vitro determination of chlorophylls a, b, c1 + c2 and pheo-pigments in marine and freshwater algae by visible spectrophotometry (Arar, 1997a); Method 447.0 - Determination of chlorophylls a and b and the identification of other pigments of interest in marine and freshwater algae using high-performance liquid chromatography with visible wavelength detection (Arar, 1997b).

Remote sensing using different algorithms for determining the Chl-a content has gained popularity (Bhagowati & Ahamad, 2019), and several authors have modeled eutrophication from nutrient loads with empirical and satellite imagery-derived models (Vinçon-Leite & Casenave, 2019), and conducted spatial and temporal monitoring (Dörnhöfer & Oppelt, 2016). However, several problems with these methods have been reported, such as atmospheric correction (Zheng & DiGiacomo, 2017; Majozi, Salama, Bernard, Harper, & Habte, 2014), atmospheric re-absorption of fluorescence (Meroni *et al*., 2009), potential inaccuracies due to the low angle of incidence of sunlight during several months of the year (Harvey, Kratzer, & Phillipson, 2015), inadequate spatial resolution for small water bodies (Qi, Hu, Duan, Cannizzaro, & Ma, 2014), chlorophyll re-absorbing effects (Gitelson,

Tecnología y ciencias del agua, ISSN 2007-2422, 13(5), 101-135. DOI: 10.24850/j-tyca-13-05-04

Buschmann, & Lichtenthaler, 1998), and saturation of reflectance (Gitelson, Buschmann, & Lichtenthaler, 1999).

Satellite sensors frequently used for estimating Chl-a include the Landsat series, with a spatial resolution of 30 m (NASA, 2018); MERIS, with a spatial resolution of 300 m (ESA, 2011); MODIS, with a spatial resolution of 1000 m; VIIRS, with a spatial resolution of 375-750 m (SPORT, 2018); and SeaWiFS, with a spatial resolution of 4 km (OceanColor, 2018).

Vegetation absorbs different wavelengths of incident sunlight energy by photosynthetic pigments (chlorophylls, carotenoids, and phycobilins), which are then used in photosynthesis. However, some incident energy is not used, and the remaining energy is either transformed into heat or re-irradiated as fluorescence (Rost, 1996). When pigments are extracted in solvents, fluorescence and absorption spectra exhibit a red shift changing their peaks by nearly 20nm depending on the solvent used. It has been previously reported that Chl-a extracted in ethyl alcohol shows an absorption peak at 662nm (Fabrowska, Messyasz, Walkowiak, Szyling, & Leska, 2017; Aguirre-Gomez, Weeks, & Boxal, 2001) while in-vivo has been reported close to 680 nm (Zucchelli *et al*., 2002; Aguirre-Gomez *et al*., 2001).

Certain wavelengths of incident sunlight are absent or significantly attenuated (Fraunhofer lines) as they are absorbed by the sun's chromatosphere or the Earth's atmosphere. Therefore, incident light and its reflections of those wavelengths are also expected to be attenuated.

Tecnología y ciencias del agua, ISSN 2007-2422, 13(5), 101-135. DOI: 10.24850/j-tyca-13-05-04

Vegetation fluorescence can then be detected at those precise wavelengths with a higher signal-to-noise ratio (SNR). Fraunhofer lines have been used to passively measure the sun-induced fluorescence (SIF) from vegetation (Plascyk & Gabriel, 1975), and, using the same principles, Moya *et al*. (2004) proposed a new remote sensing device (Moya *et al*., 2004).

The Fraunhofer line produced by terrestrial oxygen absorption at 686.7 nm is often used to measure SIF, as the Chl-a fluorescence peaks are located at approximately 685 nm. However, this line is also very close to the Chl-a absorption peak at 680 nm, which can cause undesirable effects, such as nonlinear fluorescence emission and self-absorption, at higher concentrations of Chl-a. Fraunhofer lines produced by terrestrial oxygen/water vapor absorption in the far-red band (720-730 nm) have also been previously used to measure SIF, as there is no re-absorption effect band. However, the sensitivity of image sensors at those wavelengths (5-20 %) is lower than their sensitivity to the red band (60-80 %), and commercial-grade image sensor/lens systems typically cut those wavelengths using a built-in infrared cut filter (Gitelson *et al*., 1998).

This study explores the detection of SIF at the Hα Fraunhofer line located at 656.3 nm, where the re-absorption effect is less significant, and the sensitivity of image sensors is still high. The objectives of this investigation were to: determine the feasibility of a narrow-band optical filter (NBF) coupled with an image sensor for estimating the Chl-a concentration; establish a method to determine the best regression

Tecnología y ciencias del agua, ISSN 2007-2422, 13(5), 101-135. DOI: 10.24850/j-tyca-13-05-04

model for obtaining images of Chl-a, and provide methods for monitoring and managing small lakes.

Materials and methods

Materials

Two types of digital cameras were used for image acquisition: Zenmuse X3 and Zenmuse X5, which were mounted on a Matrice 600 drone. These devices were all from the brand DJI. The cameras were coupled/decoupled with an NBF with a central wavelength of approximately 656.3 nm to acquire the narrow-band imagery and RGB, respectively.

The Camera Zenmuse X3 (part #FC350H) contained a Sony complementary metal-oxide-semiconductor (CMOS) ExmorR color image sensor (IMX377), which achieves excellent image noise reduction using the Sony pixel backlight technology and correlated double sampling (CDS). The sensor size is 6.17 x 4.55 mm with a resolution of

Tecnología y ciencias del agua, ISSN 2007-2422, 13(5), 101-135. DOI: 10.24850/j-tyca-13-05-04

4000×3000. The camera lens system has a field of view of 94º, and the camera has a fixed aperture of f/2.8 and a focus distance of 20 mm.

The camera Zenmuse X5 contained a Sony CMOS Exmor color image sensor (IMX159), which had a 17.3/13.0 mm size with 16.0M effective pixels. A DJI MFT 15-mm camera lens system was used, with three aspherical elements and a field of view of 72º. This camera has a variable aperture from f/1.7 to f/16, an ISO range of 100-25600, an electronic shutter speed of 8-1/8 000 s, a maximum image size of 4 608 × 3 456, and a focus distance of 30 mm.

The relative spectral sensitivities of the DJI X3 and X5 image sensors are shown in Figure 1.

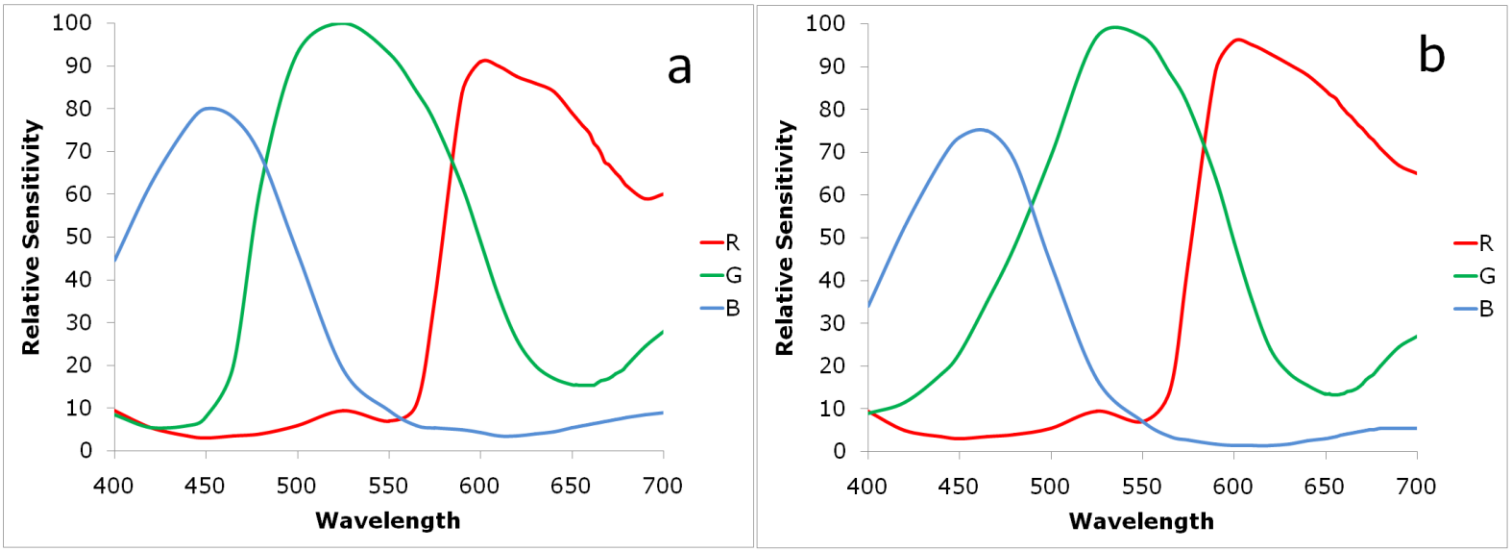

Figure1. Relative spectral sensitivity: a) image sensor on DJI X3; b) image sensor on DJI X5.

The Narrow-band filter (NBF) used in this study was a two-cavity high-transmittance filter manufactured by Andover inc., which reported a center wavelength of 660.99 nm, full width at half maximum of 9.74 nm, and a transmission peak of 82.06 %. This filter meets the requirements of quality grade 80-50 listed in MIL-PRF-13830B.

The spectral transmittance chart of the filter Is shown in Figure 2a, and spectral responses for cameras X3 and X5 when coupled with this filter are shown in Figure 2b and 2c, respectively. Only the red-band information was usable when the cameras were coupled with this filter.

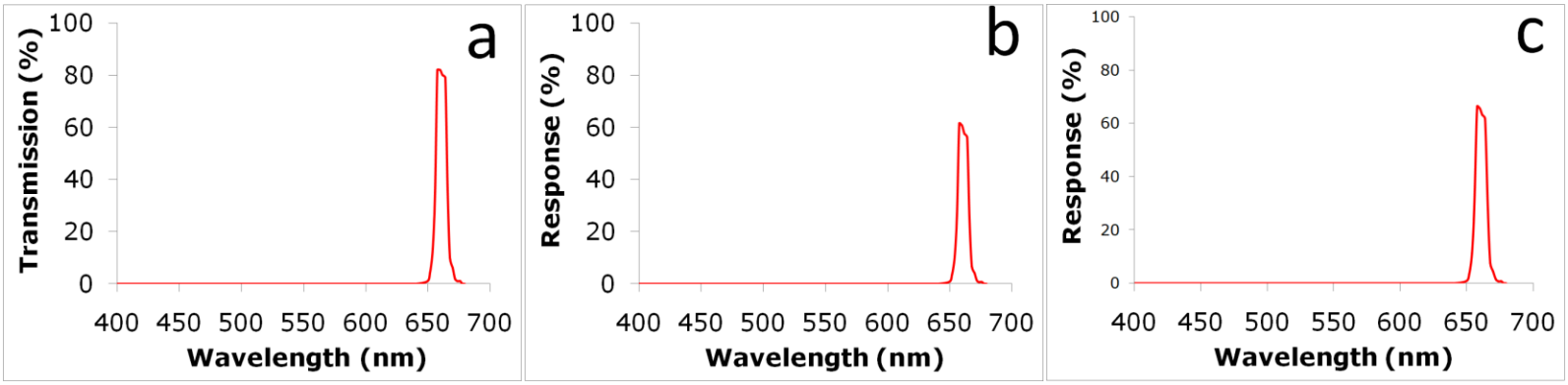

Figure 2. a) Transmission data reported by the filter manufacturer and the filter's expected response in the red band on b) X3 and c) X5.

Methods

Tecnología y ciencias del agua, ISSN 2007-2422, 13(5), 101-135. DOI: 10.24850/j-tyca-13-05-04

Tecnología y Ciencias del Agua

OPEN ACCESS

Check for updates

The study was conducted in the El Rejón Reservoir in Chihuahua City, Mexico. The reservoir was divided into two sections (A and B), and 10 points numbered from P1-P10 were distributed throughout the reservoir for sample collection to determine the Chl-a concentration in the laboratory determination (Figure 3).

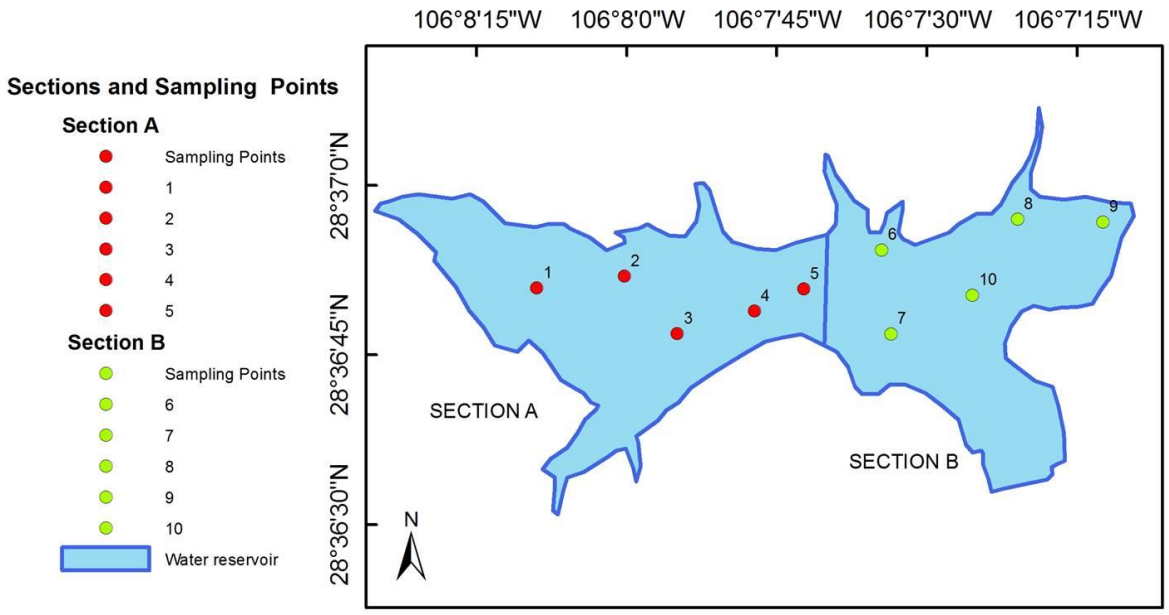

Figure 3. El Rejón reservoir study area and the distribution of sampling points. The map was created using the ArcGIS® software by Esri.

The images were acquired within the same hour, at approximately 08:30, 60 m above the water surface under clear sky conditions and 20 °C. The ISO and fixed exposure times were 100 and 1/80 or 1/5000 s for capturing the 660 nm and RGB images, respectively. The raw file type was selected (DNG) to prevent information loss by compression artifacts. Automatic GPS waypoints flights secured the spatial repeatability of images acquired between sessions at a fixed altitude and orientation with automatic camera shooting. All relevant information was embedded in the metadata of the images.

Water samples were collected from the photic zone on August 19th, 2018, following the methods described in EPA (2000) and Method 445.0 and laboratory indications (Arar & Collins, 1997). The samples were transported in dark bottles to prevent exposure to light and stored in ice immediately after collection. Approximately 250 ml of each water sample was vacuum-filtered within 4 hours of collection through Whatman 934-AH glass microfiber filters with a diameter of 47 mm. The vacuum conditions never exceeded the recommended values (10 minutes at -20.32 kPa). Finally, the filters were bent and enveloped in aluminum foil,, frozen, packed with refrigerant gel, and then shipped to arrive in the laboratory within 24 hours

Images were acquired in three sessions. The first session was conducted on August 19th, 2018, for both sections and used the X3 camera for the 660-nm band. The second and third sessions were conducted on August 24th and 25th, 2018, for sections A and B,

Tecnología y ciencias del agua, ISSN 2007-2422, 13(5), 101-135. DOI: 10.24850/j-tyca-13-05-04

respectively, during which camera X5 was used to capture the 660-nm and RGB bands.

The acquired images were initially processed using the Raw Studio 2.0 open-source software. The processing steps included luminance equalization between sessions with reference images, trans-codification from the DNG file format to .tif, and copying the metadata from the original files to the post-processed images. The .tif images were sub-sampled to determine the pixel-sensed light levels using ArcGIS® 10.2.1 for Desktop, with a pattern of 30 points randomly distributed in the proximity of the physical water sample. The same pattern was used to extract data from all images. A total of 300 tabular data points (10 images, 30 subsamples per image) were exported in a CSV file.

The selection of raw data image files and later workflow processing preserved the original numerical values the image sensor got from the upwelling photons collected within each pixel, either with the built-in Bayer filter (RGB) presented in Figure 1 or with the superposed NBF shown in Figure 2. Therefore, the 300-pixel values used in this statistical evaluation are direct representations of the water body's reflection-emission patterns at the wavelengths of interest.

The CSV file containing the 300-pixel values was processed using the Minitab® 17 statistical software (Minitab Inc., State College, PA, USA). A variance (ANOVA) analysis was conducted to determine whether the NBF was sufficiently sensitive to distinguish the pixel-sensed values between sampling points. The linear regression of the Chl-a

Tecnología y ciencias del agua, ISSN 2007-2422, 13(5), 101-135. DOI: 10.24850/j-tyca-13-05-04

concentrations and pixel values under the 660-nm band was calculated to evaluate whether this band could be a good estimator of Chl-a, and a linear regression was also conducted that included all available bands to improve the correlation.

The regression model was entered into ArcGIS® 10.2.1 for Desktop to map the Chl-a concentration in the water reservoir using spline interpolation.

Results

The laboratory-reported Chl-a concentrations are shown in Figure 4. The highest concentrations of 173.0, 128.0, 96.3, 96.7, and 171.0 µg/l were measured at sites P1, P2, P3, P5, and P9, respectively.

Tecnología y ciencias del agua, ISSN 2007-2422, 13(5), 101-135. DOI: 10.24850/j-tyca-13-05-04

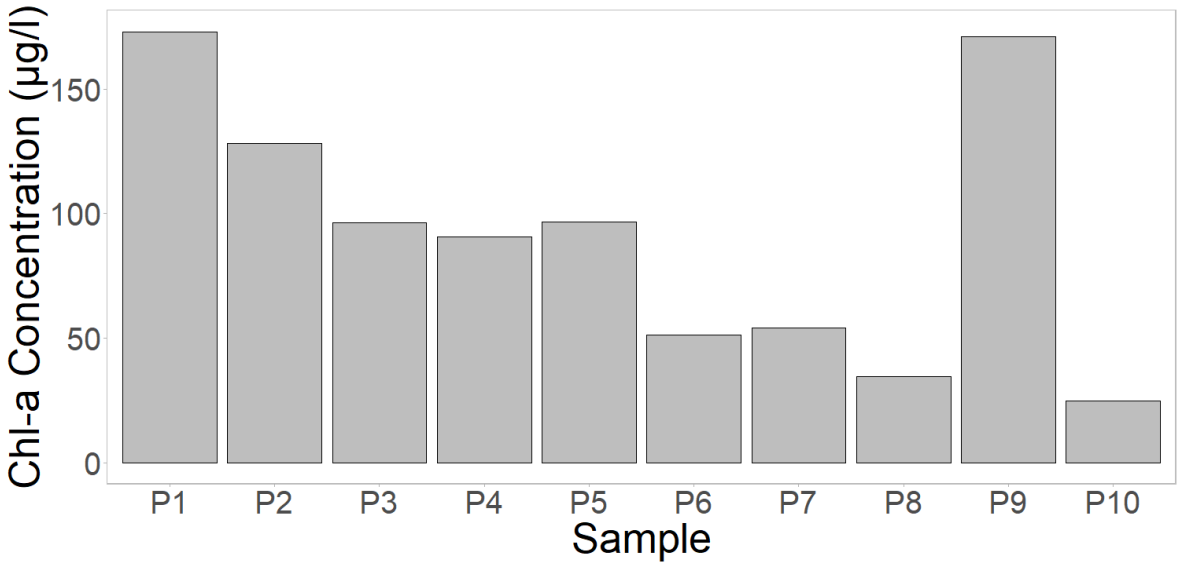

Figure 4. Chl-a concentration reported by the laboratory for all sampling points.

An ANOVA test (p = 0.000) confirmed that camera X3 coupled with a 660-nm narrow-band filter could distinguish between the sampling points well. The Tukey comparisons show seven statistically different groups, indicated by letters A to G in Table 1.

Table 1. Results of the ANOVA test and Tukey comparisons for the X3 pixel value at 660 nm by sampling site.

Tecnología y ciencias del agua, ISSN 2007-2422, 13(5), 101-135. DOI: 10.24850/j-tyca-13-05-04

Sampling site	Mean	95 % CI of a pixel value	SE Mean	St. Dev.	Tukey Grouping						
P1	71.733	(70.044, 73.423)	0.897	4.913	A						
P2	62.933	(61.244, 64.623)	0.896	4.906		B					
P3	47.667	(45.977, 49.356)	0.661	3.623			C				
P4	47.233	(45.544, 48.923)	0.575	3.148			C				
P5	41.833	(40.144, 43.523)	0.591	3.239				D	E		
P6	43.167	(41.477, 44.856)	0.675	3.696				D			
P7	38.2	(36.511, 39.889)	0.766	4.197					E	F	
P8	37.5	(35.81, 39.19)	1.39	7.61						F	
P9	33.2	(31.511, 34.889)	0.945	5.176							G
P10	37.6	(35.911, 39.289)	0.884	4.839						F	

An ANOVA test (p = 0.000) also confirmed that camera X5 coupled with a 660-nm narrow-band filter could distinguish between the sampling points well. The Tukey comparisons show six statistically different groups, marked A to F in Table 2.

Tecnología y ciencias del agua, ISSN 2007-2422, 13(5), 101-135. DOI: 10.24850/j-tyca-13-05-04

Table 2. Results of the ANOVA test and Tukey comparisons for the X5 pixel values at 660 nm by sampling site.

Sampling site	Mean	95 % CI of a pixel value	SE Mean	St. Dev.	Tukey Grouping						
P1	51.567	(51.069, 52.065)	0.218	1.194	A						
P2	39.033	(38.535, 39.531)	0.273	1.497		B					
P3	30.9	(30.402, 31.398)	0.232	1.269			C				
P4	28.467	(27.969, 28.965)	0.208	1.137				D			
P5	26.767	(26.269, 27.265)	0.261	1.431					E		
P6	30.033	(29.535, 30.531)	0.33	1.81			C				
P7	26.467	(25.969, 26.965)	0.287	1.57					E		
P8	26.833	(26.335, 27.331)	0.152	0.834					E		
P9	25.933	(25.435, 26.431)	0.262	1.437					E	F	
P10	25.1	(24.602, 25.598)	0.264	1.447						F	

An ANOVA test (p = 0.000) indicated that camera X5 could not distinguish the sampling points well without a filter. The Tukey comparisons show three statistically different groups marked A to C in Table 3.

Tecnología y ciencias del agua, ISSN 2007-2422, 13(5), 101-135. DOI: 10.24850/j-tyca-13-05-04

Table 3. ANOVA test and Tukey comparison results for the X5 pixel values with no filter by sampling site.

Sampling site	Mean	95 % CI of a pixel value	SE Mean	St. Dev.	Tukey Grouping						
P1	14.333	(13.602, 15.064)	0.515	2.82	A						
P2	5.267	(4.536, 5.998)	0.64	3.503		B					
P3	1.167	(0.436, 1.898)	0.288	1.577			C				
P4	0.9	(0.169, 1.631)	0.277	1.517			C				
P5	0.233	(-0.498, 0.964)	0.104	0.568			C				
P6	0.833	(0.102, 1.564)	0.23	1.262			C				
P7	0.267	(-0.464, 0.998)	0.126	0.691			C				
P8	0.7	(-0.031, 1.431)	0.215	1.179			C				
P9	12.733	(12.002, 13.464)	0.621	3.403	A						
P10	0.4	(-0.331, 1.131)	0.183	1.003			C				

The red band in the RGB images could not distinguish between sites P3, P4, P5, P6, P7, P8, and P10, all statistically grouped into C. In contrast, the images captured by X3 and X5 with the 660-nm filter could differentiate these sampling points well, as they were categorized into five and four different groups, respectively.

Tecnología y ciencias del agua, ISSN 2007-2422, 13(5), 101-135. DOI: 10.24850/j-tyca-13-05-04

The water column at P9 was identified as different. With the 660-nm filter, the images from both cameras showed a decrease in the mean pixel value from site P8 to P9 (-11.5 % and -3.3 % for cameras X3 and X5, respectively). In comparison, there was a significant increase (+1 700 %) in the mean pixel value for the red band in the RGB image. This increase was not due to an increase in the Chl-a, as no increase in fluorescence was sensed at 660 nm. Therefore, P9 was removed from further analysis to prevent this value from skewing the entire regression model to fit a value that would not have corresponded to Chl-a.

Simple linear regression (SLR) analysis, in the form of $Y = \beta_0 + \beta_1 *X$, showed that the 660-nm narrow-band filter could estimate the Chl-a concentration well, with R^2 values of 0.86 and 0.77 for cameras X3 and X5, respectively, with a normal probability of residuals for random errors (Figure 5). This could be because the X3 images were acquired on the same day as the water samples, while the X5 images were captured one week later. The R^2 of the regular *R* image (no filter installed) was 0.68.

Tecnología y ciencias del agua, ISSN 2007-2422, 13(5), 101-135. DOI: 10.24850/j-tyca-13-05-04

Tecnología y Ciencias del Agua

OPEN ACCESS

Check for updates

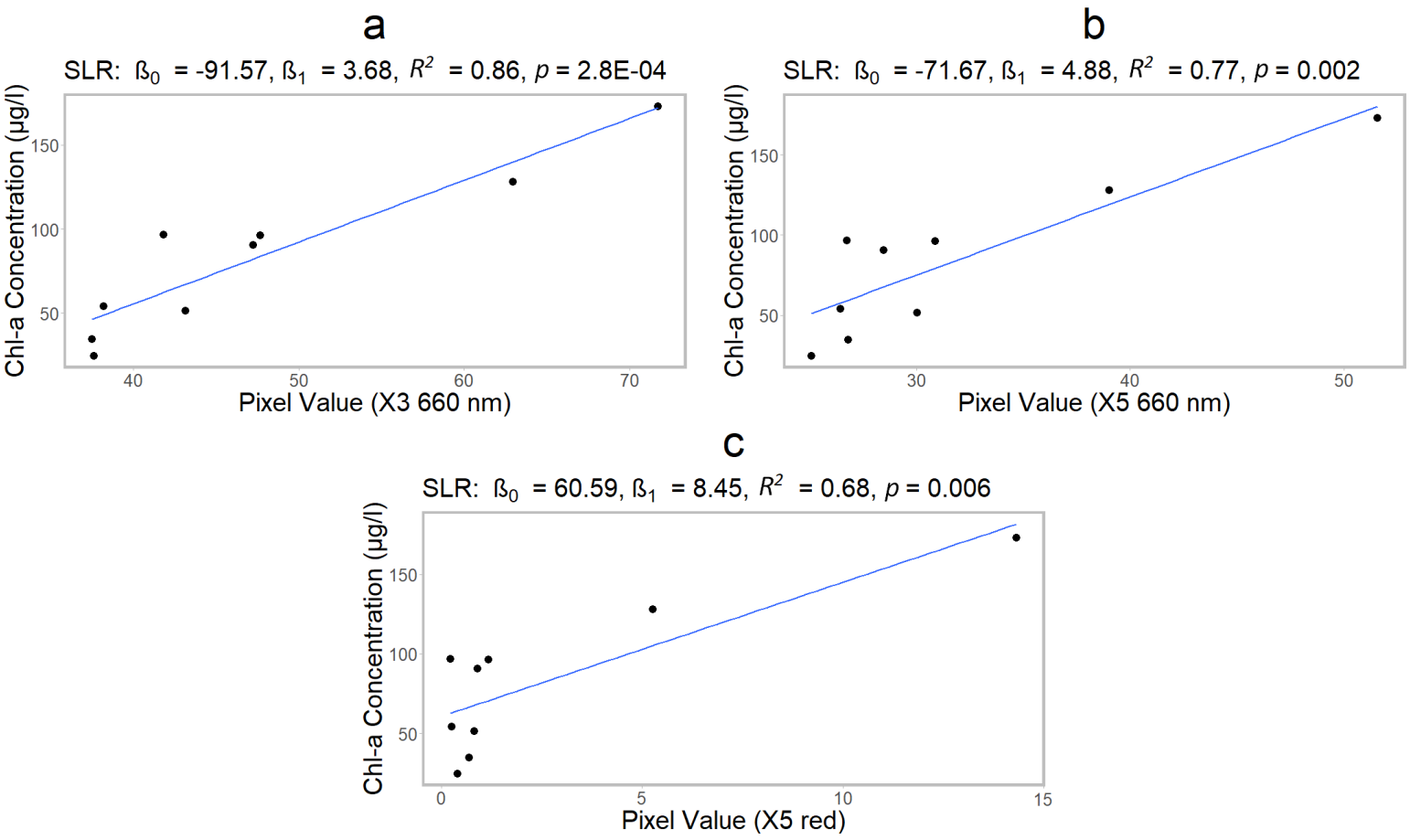

Figure 5. Simple regression model of the mean pixel values against the Chl-a concentration: a) X3 660 nm; b) X5 660 nm; c) X5 red.

Figures 5a, 5b, and 5c show that *p*-values for all SLRs were lower than 0.05. Additionally, the normality of models' residuals was confirmed with a Shapiro-Wilk normal test with *p*-values of 0.59, 0.45, and 0.28, respectively.

The R^2 values of the multiple regressions conducted using over one band did not greatly increase, while the model's capacity to predict new values was greatly impacted (*R*-sq *p*red; Table 4). Therefore, the simple regression conducted using the 660-nm band was considered the best model.

Table 4. Multiple regression analysis listing the two most suitable models when using one to five variables (Vars). X indicates the variables used in each model.

Vars	R-Sq	R-Sq (adj)	R-Sq (pred)	Mallows Cp	S	X3 R660	X5 R660	X5R RGB	X5G RGB	X5B RGB
1	0.864	0.845	0.805	-1.3	18.76	X				
1	0.838	0.815	0.757	-0.6	20.495					X
2	0.872	0.829	0.45	0.5	19.679	X	X			
2	0.869	0.825	0	0.6	19.919	X		X		
3	0.885	0.815	0.65	2.1	20.464	X			X	X
3	0.873	0.797	0	2.5	21.477	X	X	X		
4	0.888	0.777	0.131	4	22.516	X	X		X	X
4	0.886	0.772	0	4.1	22.729	X		X	X	X
5	0.89	0.706	0	6	25.818	X	X	X	X	X

The best model, Chl-a = -91.71+ 3.680*(X3 R660), was entered into ArcGIS® 10.2.1 for Desktop, and the Chl-a concentrations were

Tecnología y ciencias del agua, ISSN 2007-2422, 13(5), 101-135. DOI: 10.24850/j-tyca-13-05-04

estimated and interpolated over the entire reservoir. The water reservoir area located in the northwest receives water from El Rejón Stream and had the highest concentration of Chl-a, decreasing in concentration towards the southeast of the reservoir (Figure 6). This behavior could be explained by the run-off of nutrients from upstream agricultural activities.

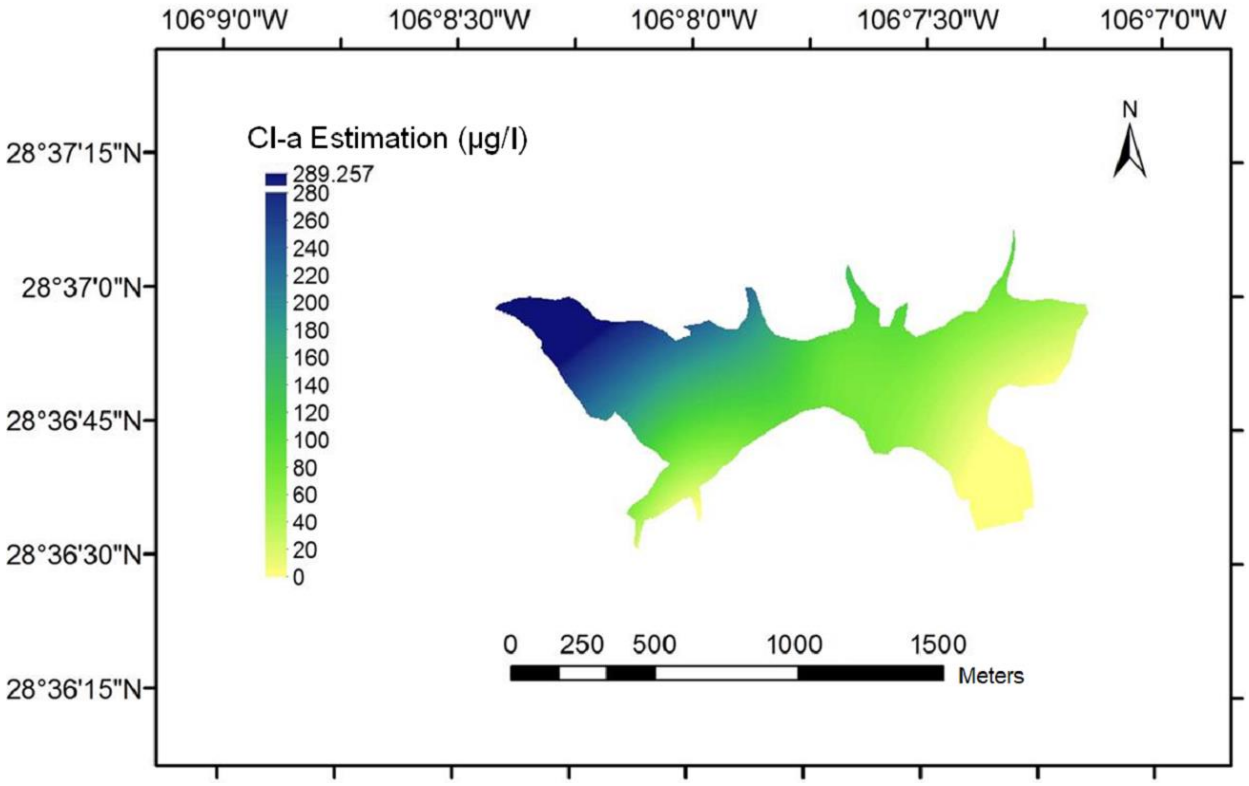

Figure 6. Estimation and distribution of Chl-a. This map was created using ArcGIS®.

Tecnología y ciencias del agua, ISSN 2007-2422, 13(5), 101-135. DOI: 10.24850/j-tyca-13-05-04

Discussion

The regression equations against the Chl-a concentrations for the images captured at 660 nm by both cameras exhibited positive slopes (3.680 & 4.888, respectively), indicating an increase in the response of the pixel values with an increase in the Chl-a concentration. Both R^2 values were high (0.86 & 0.77, respectively), and their residuals were normally distributed. Therefore, this was a good mathematical model for estimating Chl-a.

Under in-vivo conditions, no significant fluorescence of chlorophylls b or c has been observed, and the total fluorescence was mainly dominated by Chl-a as reported by other authors (Rost, 1996). However, under in-vitro conditions, almost all photosynthetic pigments, excluding carotenoids, exhibited fluorescence (DeEll & Toivonen, 2003). The presence of such pigments will cause the fluorescence bands of different chlorophyll pigments and other water column components in the spectrum's red region to overlap (Arar & Collins, 1997). This occurred at P9, where incident sunlight was reflected, scattered, and sensed in the regular red band, which increased the mean pixel value (+1 719 %) from 0.7 at P8 to 12.733 in P9. These increased emissions were not sensed in the upwelling light at 660 nm by camera X3, which

Tecnología y ciencias del agua, ISSN 2007-2422, 13(5), 101-135. DOI: 10.24850/j-tyca-13-05-04

sensed a decrease (-11.4 %) in the mean pixel value from 37.5 at P8 to 33.2 at P9. The results of camera X5 were similar - a decrease (-3.3 %) in the mean pixel value from 26.833 at P8 to 25.933 at P9 was observed. Therefore, the increase was not due to an increase in the Chl-a; rather, it was due to the presence of other components in the water column that presented fluorescence at 660 nm after they were dissolved in acetone, which affected the laboratory results. Therefore, the narrow-band filter used in this investigation (660 nm) could distinguish between Chl-a and other components during in-vivo measurement, while in-vitro measurements could not.

The methodology presented here has advantages over satellite and airborne remote sensing as no significant atmospheric corrections are required when images are captured at the height of 60 m, which overcomes several of the issues reported by other authors, including the lack of adequate atmospheric correction algorithms for all wavelengths (Majozi *et al*., 2014), the requirement for complex atmospheric correction models (Simis *et al*., 2007), inaccuracies due the presence of aerosols in the high atmosphere (Hyde, O'Reilly, & Oviatt, 2007), and adjacent land interference (Simis *et al*., 2007).

Other authors have investigated sun-induced fluorescence, particularly in the Fraunhofer lines at wavelengths of 656.3, 687, and 735 nm (Moya *et al*., 2004; Le *et al*., 2013; Verrelst *et al*., 2016), and others have estimated the Chl-a concentration in water bodies at wavelengths ranging from 660 to 665 nm (Simis *et al*., 2007; Mathews, Stewart, & Winter, 2010; Smith, Lain, & Bernard, 2018; Zeng,

Richardson, & King, 2017; Stratoulias, Balzter, Zlinszk, & Tóth, 2015; Le *et al*., 2013).

The R^2 value of the regression model reported in this study for estimating the Chl-a concentration using an image sensor and NBF centered at 660 nm was 0.86. Bohn *et al*. (2018) reported R^2 values ranging from 0.72 to 0.77 when estimating the Chl-a concentration from satellite images captured by Landsat 7 (Bohn *et al*., 2018), while Stratoulias *et al*. (2015) reported an R^2 value of 0.76 when estimating the Chl-a concentration from airborne hyper-spectral images (Stratoulias *et al*. 2015).

Tung-Ching reported an R^2 value of 0.68 when estimating Chl-a from multispectral imagery with visible and infrared bands captured by a drone (Tung-Ching, 2017), and Zeng *et al*. reported an R^2 value of 0.87 when estimating the Chl-a from images captured at a band ratio of 685:665 nm with two spectrometers for down-welling radiation from the sun and upwelling radiation from the water's surface (Zeng *et al*., 2017).

The use of NBF with Full width at half maximum of 9.74 nm allowed to sense the upwelling sun-induced fluorescence; it contains a certain degree of error since it still senses reflection of wavelengths below and above Hα (656.3 nm). This method could be improved by using even closer wavelength bandwidths; however, it would require active temperature controls on the filter to prevent shifts in center wavelength producing inaccurate results.

Tecnología y ciencias del agua, ISSN 2007-2422, 13(5), 101-135. DOI: 10.24850/j-tyca-13-05-04

The constant motion of the water surface combined with the lense's narrow field of view limited the possibility of producing ortho-mosaic photos and directly a Chl-a map solely from the imagery; thus, it needed to be interpolated using the spline method. Wider field of view lenses and spatial corrections are recommended for future studies.

Conclusion

The Chl-a concentration could be better estimated using a narrow-band filter than an RGB sensor for any other band, with a maximum R^2 value of 0.86. The methodology presented here could remove interference from other water column components. The 661-nm band alone could better predict Chl-a than any other RGB band, and its performance was better than most previous studies. Multiple regression analysis did not improve the ability of the model to predict new values. Therefore, simple regression analysis was most suitable for mapping Chl-a. Thus, this methodology is adequate for monitoring and managing small lakes.

While this study shows an excellent correlation coefficient between imagery data and Chl-a concentrations obtained from laboratory analysis, the image acquisition sessions were carefully selected to

Tecnología y ciencias del agua, ISSN 2007-2422, 13(5), 101-135. DOI: 10.24850/j-tyca-13-05-04

isolate the variations from the ones caused by the NBF from other factors (angle of light incidence, water surface reflections, NBF's temperature, cloud effects), the result of those controlled conditions was quite evident on the image equalization process where negligible or no corrections were required. Further exploration of the effects caused by those factors is set to be studied in future research. At the same time, it is highly recommended to equalize the images among sessions to compensate for variations in those conditions during surveys.

Acknowledgments

The authors greatly acknowledge the financial support of the Program for Teaching Professional Development for the Higher Type (PRODEP) (Agreement UACH-PTC-354, number 511-6 / 17-8204).

References

Aguirre-Gomez, R., Weeks, A., & Boxal, S. (2001). The identification of phytoplankton pigments from absorption spectra. International *Journal of Remote Sensing*, 315-338. DOI: 10.1080/014311601449952

Arar, E. J. (1997a). *Method 446.0: In vitro determination of chlorophylls a, b, c + c and pheopigments in 1 2marine and freshwater algae by visible spectrophotometry*. Washington, DC, USA: U.S. Environmental Protection Agency.

Arar, E. J. (1997b). *Determination of chlorophylls a and b and identification of other pigments of interest in marine and freshwater algae using high performance liquid chromatography with visible wavelength detection*. Washington, DC, USA: U.S. Environmental Protection Agency.

Arar, E. J., & Collins, G. B. (1997). *Method 445.0 in vitro determination of chlorophyll and pheophytin ain marine and freshwater algae by fluorescence*. Washington, DC, USA: U.S. Environmental Protection Agency. DOI: EPA-822-B00-001

Bhagowati, B., & Ahamad, K. U. (2019). A review on lake eutrophication dynamics and recent developments in lake modeling. *Ecohydrology & Hydrobiology*, 19(1), 155-166. DOI: 10.1016/j.ecohyd.2018.03.002

Bohn, V. Y., Carmona, F., Rivas, R., Lagomarsino, L., Diovisalvi, N., & Zagarese, H. E. (2018). Development of an empirical model for chlorophyll-a and secchi disk depth estimation for a Pampean shallow lake (Argentina). *The Egyptian Journal of Remote Sensing and Space Sciences*, 21(21), 183-191. DOI: 10.1016/j.ejrs.2017.04.005

Chen, X., Chen, Y., Shimizu, T., Niu, J., Nakagami, K., Qian, X.,..., & Li, J. (2017). Water resources management in the urban agglomeration of the Lake Biwa region, Japan: An ecosystem services-based sustainability assessment. *Science of the Total*

Environment, 586, 174-187. DOI: 10.1016/j.scitotenv.2017.01.197

DeEll, J. R., & Toivonen, P. M. (2003). In: Food, O. M. (ed.). *Practical applications of chlorophyl fluorescence*. Simcoe, Canada: Springer Science + Business Media New York. DOI: 10.1007/978-1-4615-0415-3

Dörnhöfer, K., & Oppelt, N. (2016). Remote sensing for lake research and monitoring – Recent advances. *Ecological Indicators*, 64, 105-122. DOI: 10.1016/j.ecolind.2015.12.009

EPA, Environmental Protection Agency. (2000). Nutrient criteria technical guidance manual, lakes and reservoirs. Washington, DC, USA: U.S. Environmental Protection Agency.

ESA, European Space Agency. (2011). *Meris products specifications*. Recovered from https://earth.esa.int/documents/700255/707222/Vol11_Meris_6a.pdf

Fabrowska, J., Messyasz, B., Walkowiak, J., Szyling, J., & Leska, B. (2017). Isolation of chlorophylls and carotenoids from freshwater algae using different extraction methods. *Phycological Research*, 66(1), 52-57. DOI: 10.1111/pre.12191

Gitelson, A. A., Buschmann, C., & Lichtenthaler, H. K. (1999). The chlorophyll fluorescence ratio F735/F700 as an accurate measure of the chlorophyll content in plants. *Remote Sensing of Environment*, 69(3), 296-302.

Gitelson, A. A., Buschmann, C., & Lichtenthaler, H. K. (1998). Leaf chlorophyll fluorescence corrected for re-absorption by means of absorption and reflectance measurements. *Journal of Plant Physiology*, 152(2-3), 283-296.

Harvey, E. T., Kratzer, S., & Phillipson, P. (2015). Satellite-based water quality monitoring for improved spatial and temporal retrieval of chlorophyll-a in coastal waters. *Remote Sensing of Environment*, (158), 417-430. DOI: http://dx.doi.org/10.1016/j.rse.2014.11.017

Henny, C., & Meutia, A. (2014). Urban lakes in Megacity Jakarta: Risk and management plan for future sustainability. *Procedia Environmental Sciences*, 20, 737-746. DOI: 10.1016/j.proenv.2014.03.088

Hyde, K. J., O'Reilly, J. E., & Oviatt, C. A. (2007). Validation of SeaWiFS chlorophyll a in Massachusetts Bay. *Continental Shelf Research*, 27(12), 1677-1691. DOI: 10.1016/j.csr.2007.02.002

Khorasani, H., Kerachian, R., & Malakpour-Estalakia, S. (2018). Developing a comprehensive framework for eutrophication management in off-stream artificial lakes. *Journal of Hydrology*, 562, 103-124. DOI: 10.1016/j.jhydrol.2018.04.052

Le, C., Hu, C., Cannizzaro, J., English, D., Muller-Karger, F., & Lee, Z. (2013). Evaluation of chlorophyll-a remote sensing algorithms for an optically complex estuary. *Remote Sensing of Environment*, 129, 75-89. DOI: http://dx.doi.org/10.1016/j.rse.2012.11.001

Majozi, N. P., Salama, M. S., Bernard, S., Harper, D. M., & Habte, M. G. (2014). Remote sensing of euphotic depth in shallow tropical inland waters of Lake Naivasha using MERIS data. *Remote Sensing of Environment*, (148). DOI: http://dx.doi.org/10.1016/j.rse.2014.03.025

Mathews, M., Stewart, B., & Winter, K. (2010). Remote sensing of cyanobacteria-dominant algal blooms and Water quality parameters in Zeekoevlei, a small hypertrophic lake, using MERIS. *Remote Sensing of Environment*, 114(9), 2070-2087. DOI: 10.1016/j.rse.2010.04.013

Meroni, M., Rossini, M., Guanter, L., Alonso, L., Rascher, U., Colombo, R., & Moreno, J. (2009). Remote sensing of solar-induced chlorophyll fluorescence: Review of methods and applications. *Remote Sensing of Environment*, 113(10), 2037-2051. DOI: 10.1016/j.rse.2009.05.003

Moya, I., Camenen, L., Evain, S., Goulas, Y., Cerovic, Z. G., Latouche, G...., & Ounis, A. (2004). A new instrument for passive remote sensing. Measurements of sunlight-induced chlorophyll fluorescence. *Remote Sensing of Environment*, 91(2), 186-197. DOI: 10.1016/j.rse.2004.02.012

NASA. (2018). *Landsat 8*. Recovered from https://landsat.gsfc.nasa.gov/

Natarajan, S. K., Hagare, D., & Maheshwari, B. (2018). Understanding socio-economic benefits of stormwater management system

through urban lakes in Western Sydney, Australia. *Ecohydrology & Hydrobiology*, 18(4), 412-419. DOI: 10.1016/j.ecohyd.2018.11.003

OceanColor. (2018). *SeaWiFS*. Recovered from https://oceancolor.gsfc.nasa.gov/data/seawifs/seastar/spacecraft/

Plascyk, J. A., & Gabriel, F. C. (1975). The fraunhofer line discriminator MKII-An airborne instrument for precise and standardized ecological luminescence measurement. *IEEE Transactions on Instrumentation and Measurement*, 24(4), 306-313. DOI: 10.1109/TIM.1975.4314448

Plisnier, P.-D., Nshombo, M., Mgana, H., & Ntakimazi, G. (2018). Monitoring climate change and anthropogenic pressure at Lake Tanganyika. *Journal of Great Lakes Research*, 44(6), 1194-1208. DOI: 10.1016/j.jglr.2018.05.019

Qi, L., Hu, C., Duan, H., Cannizzaro, J., & Ma, R. (2014). A novel MERIS algorithm to derive cyanobacterial phycocyanin pigment concentrations in a eutrophic lake: Theoretical basis and practical considerations. *Remote Sensing of Environment*, 154, 298-317. DOI: 10.1016/j.rse.2014.08.026

Rost, F. (1996). *Fluorescence microscopy* (Vol. II). Cambridge & New York, USA: Cambridge University Press. DOI: 10.1002/sca.4950180810

Simis, S. G., Ruiz-Verdú, A., Dominguez-Gomez, J., Peña-Martinez, R., Peters, S. W., & Gons, H. J. (2007). Influence of phytoplankton

pigment composition on remote sensing of cyanobacterial biomass. *Remote Sensing of Environment*, 106(4), 414-427. DOI: 10.1016/j.rse.2006.09.008

Smith, M., Lain, R. L., & Bernard, S. (2018). An optimized chlorophyll a switching algorithm for MERIS and OLCI in phytoplankton-dominated waters. *Remote Sensing of Environment*, 215, 217-227. DOI: https://doi.org/10.1016/j.rse.2018.06.002

SPORT. (2018). *VIIRS Products. SPORT, Short-term Prediction Research and Transition Center*. Recovered from https://weather.msfc.nasa.gov/sport/jpsspg/viirs.html

Stratoulias, D., Balzter, H., Zlinszk, A., & Tóth, V. (2015). Assessment of ecophysiology of lake shore reed vegetation based on chlorophyll fluorescence, field spectroscopy and hyperspectral airborne imagery. *Remote Sensing of Environment*, (157), 72-84. DOI: 10.1016/j.rse.2014.05.021

Tung-Ching, S. (2017). A study of a matching pixel by pixel (MPP) algorithm to establish an empirical model of water quality mapping, as based on unmanned aerial vehicle (UAV) images. *International Journal of Applied Earth Observation and Geoinformation*, (58), 213-224. DOI: 10.1016/j.jag.2017.02.011

Vásquez, W. F., & De-Rezende, C. E. (2018). Management and time preferences for lakes restoration in Brazil. *Science of the Total Environment*, 635, 315-322. DOI: 10.1016/j.scitotenv.2018.04.151

Verrelst, J., van der Tol, C., Magnani, F., Sabater, N., Rivera, J. P., Mohammed, G., & Moreno, J. (2016). Evaluating the predictive power of sun-induced chlorophyll fluorescence to estimate net photosynthesis of vegetation canopies: A SCOPE modeling study. *Remote Sensing of Environment*, (176), 139-151. DOI: 10.1016/j.rse.2016.01.018

Vinçon-Leite, B., & Casenave, C. (2019). Modelling eutrophication in lake ecosystems: A review. *Science of the Total Environment*, 651(2), 2985-3001. DOI: https://doi.org/10.1016/j.scitotenv.2018.09.320

Wondie, A. (2018). Ecological conditions and ecosystem services of wetlands in the Lake Tana Area, Ethiopia. *Ecohydrology & Hydrobiology*, 18(2), 231-244.

Zeng, C., Richardson, M., & King, D. (2017). The impacts of environmental variables on water reflectance measured using a lightweight unmanned aerial vehicle (UAV)-based spectrometer system. *ISPRS Journal of Photogrammetry and Remote Sensing*, 130, 217-230. DOI: https://doi.org/10.1016/j.isprsjprs.2017.06.004

Zhang, K., Yang, X., Xu, M., Lin, Q., Kattel, G., & Shen, J. (2018). Confronting challenges of managing degraded lake ecosystems in the Anthropocene, exemplified from the Yangtze River Basin in China. *Anthropocene*, 24, 30-39. DOI: 10.1016/j.ancene.2018.11.001

Zheng, G., & DiGiacomo, P. M. (2017). Remote sensing of chlorophyll-a in coastal waters based on the light absorption coefficient of phytoplankton. *Remote Sensing of Environment*, 331-341. DOI: 10.1016-j.rse.2017.09.008

Zucchelli, G., Jennings, R., Garlaschi, F., Cinque, G., Bassi, R., & Cremonesi, O. (2002). The calculated in vitro chlorophyll an absorption band shape. *Biophysical Journal*, 82, 378-390. DOI: 0006-3495/02/01/378/1